Inelastic neutron scattering studies of ^{76}Se

S. Mukhopadhyay,[1,2,*] B. P. Crider,[1,†] B. A. Brown,[3,4] A. Chakraborty,[1,2,‡] A. Kumar,[1,2,§] M. T. McEllistrem,[1] E. E. Peters,[2] F. M. Prados-Estévez,[1,2] and S. W. Yates[1,2]

[1]*Department of Physics and Astronomy, University of Kentucky, Lexington, Kentucky 40506-0055, USA*
[2]*Department of Chemistry, University of Kentucky, Lexington, Kentucky 40506-0055, USA*
[3]*National Superconducting Cyclotron Laboratory, Michigan State University, East Lansing, Michigan 48824, USA*
[4]*Department of Physics and Astronomy, Michigan State University, East Lansing, Michigan 48824, USA*

(Received 17 August 2018; revised manuscript received 20 November 2018; published 22 January 2019)

The low-lying, low-spin levels of ^{76}Se were studied with the $(n, n'\gamma)$ reaction. Gamma-ray excitation function measurements were performed at incident neutron energies from 2.0 to 3.5 MeV, and γ-ray angular distributions were measured at neutron energies of 2.4, 3.0, and 3.7 MeV. From these measurements, level spins, level lifetimes, branching ratios, and multipole mixing ratios were determined. We established the 0_2^+ band, which supports the shape coexistence in ^{76}Se predicted by large-scale shell model calculations and the interacting boson model.

DOI: 10.1103/PhysRevC.99.014313

I. INTRODUCTION

In our recent study of the nuclear structure of ^{76}Ge, which decays by two-neutrino double-β decay and is a candidate for neutrinoless double-β decay, we clarified the low-lying, low-spin level scheme using the $(n, n'\gamma)$ reaction [1]. That study was motivated by the desire to resolve questions about the level structure of ^{76}Ge and to compare the level characteristics with state-of-the-art shell model calculations. The nuclear matrix elements that govern the rate of neutrinoless double-β decay must be calculated from nuclear structure theory [2], thus it is crucial to understand the structure of the parent and daughter nuclei. In the current work, we have performed a detailed study of ^{76}Se, the double-β decay daughter of ^{76}Ge.

The stable Se nuclei exhibit a number of challenging structures, which have been interpreted as shape transitions, shape coexistence, and triaxiality [3], and ^{76}Se is typical of these nuclei with several competing features. For example, this nucleus exhibits a low-lying excited 0^+ state, an "intruder" structure typically associated with proton excitations across a shell gap, and a "γ band" with properties suggesting γ softness—i.e., a large $B(E2; 2_2^+ \rightarrow 2_1^+)$ and 3_γ^+ and 4_γ^+ levels close in energy. While a number of reactions have been used to probe the structure of ^{76}Se [4], a coherent picture has yet to emerge. The goal of the present study was to provide a comprehensive portrait of the low-energy, low-spin regime of ^{76}Se through measurements of level lifetimes, branching ratios, and multipole mixing ratios. Finally, these detailed data are compared with large-scale shell model calculations [5] and recent interacting boson model (IBM) calculations based on the Gogny energy density functional [3].

II. EXPERIMENTAL DETAILS AND DATA ANALYSIS

The ^{76}Se$(n, n'\gamma)$ experiments were performed at the University of Kentucky Accelerator Laboratory (UKAL) with the 7 MV Van de Graaff accelerator and methods described previously [6]. Protons from the accelerator were used to create nearly monoenergetic ($\Delta E \approx 60$ keV) fast neutrons via the ^{3}H$(p, n)^3$He reaction with a tritium gas target. The proton beam was pulsed at a 1.875 MHz frequency with a pulse width of approximately 1 ns. The emitted neutrons impinged upon a scattering sample, which consisted of 11.96 g of elemental selenium powder enriched to 96.95% in ^{76}Se, contained in a cylindrical polyethylene vial of 0.7 cm radius and 2.6 cm height placed at a distance of 5.7 cm from the center of the tritium gas cell where the neutrons were produced. The isotopic contaminants in the sample, as certified by the DOE Isotope Program, arise from ^{74}Se (0.19%), ^{77}Se (0.83%), ^{78}Se (0.87%), ^{80}Se (0.97%), and ^{82}Se (0.19%). Gamma rays were detected with a high-purity germanium (HPGe) detector of 50% relative efficiency and an energy resolution of 2.2 keV (FWHM) at 1333 keV surrounded by a bismuth germanate (BGO) annulus, which served as a Compton suppressor and active shield. Time-of-flight gating on the prompt γ rays reduced the background from neutron interactions in the shielding, the HPGe detector, and surrounding materials. An in-beam γ-ray spectrum obtained at 90° with respect to the beam axis at an incident neutron energy of 3.0 MeV is shown in Fig. 1.

γ-ray excitation functions were measured with a single HPGe detector at incident neutron energies between 1.6 and 3.5 MeV in steps of 100 keV at an angle of 90° relative to

*smukh3@uky.edu
†Present address: Department of Physics & Astronomy, Mississippi State University, Mississippi State, MS 39762, USA.
‡Present address: Department of Physics, Siksha Bhavana, Visva-Bharati, Santiniketan 731235, India.
§Present address: Department of Physics, Banaras Hindu University, Varanasi 221005, India.

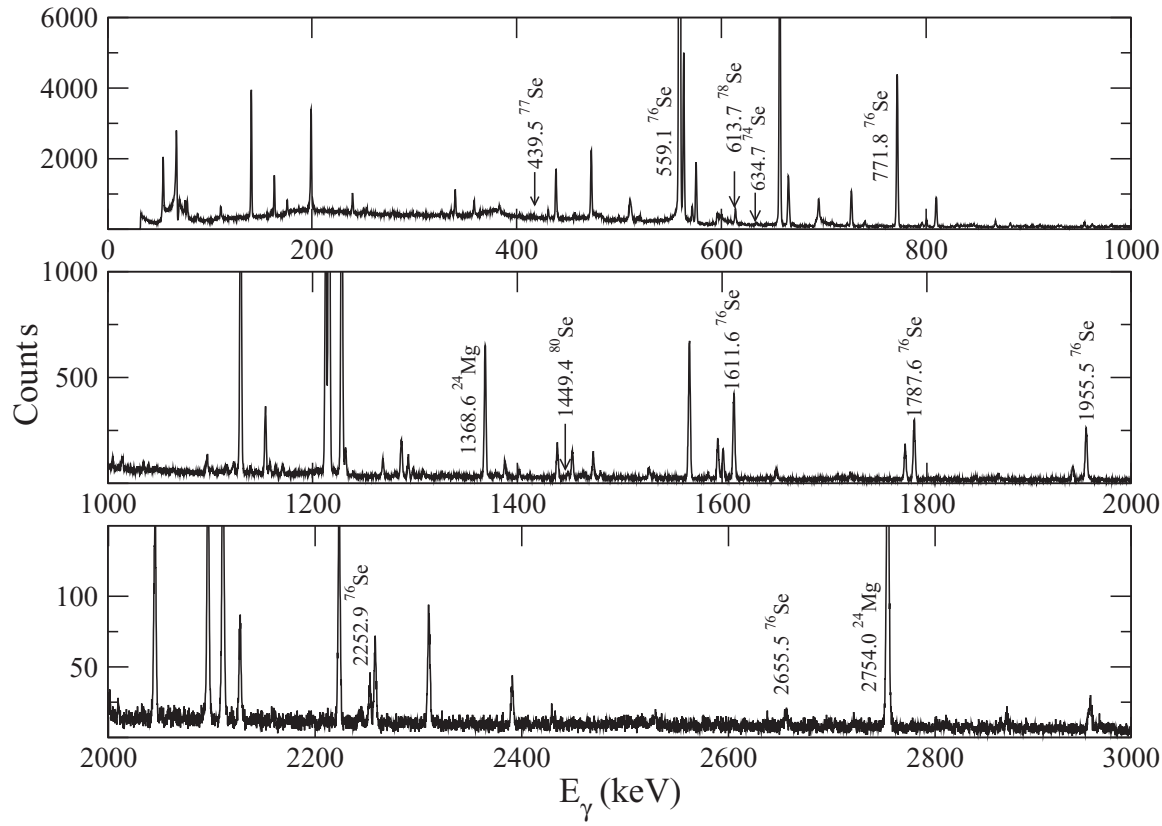

FIG. 1. γ-ray spectrum from 3.0 MeV neutrons incident on the enriched ^{76}Se scattering sample. Some prominent peaks are identified. A ^{24}Na radioactive source was placed near the detector to provide an online calibration. The two prominent γ rays arising from this source are labeled as ^{24}Mg.

the beam axis. These measurements provide γ-ray yields as a function of neutron energy, which help to determine the energy threshold for the emitting level. In addition, the relative experimental level cross sections can be compared with the theoretical cross sections computed with a statistical model code, CINDY [7], to infer the spins of the levels. An example of the spin assignment made by comparing the observed cross sections for the 2604.1 keV level with the calculated values is shown in Fig. 2.

Angular distributions of the γ rays were measured at incident neutron energies of 2.4, 3.0, and 3.7 MeV, where the emitted γ rays were detected at eleven angles from 40° to 150° relative to the beam axis. At low incident neutron energies, the inelastic neutron scattering reaction occurs predominantly through compound nucleus formation. As this reaction leads to an alignment of the excited nuclei, the angular distributions of γ rays from the decays of the excited levels exhibit anisotropies reflecting this alignment, the spins of the levels, and the multipolarities of the transitions. The variation of the yield of a particular γ ray with detection angle can be fitted with a least-squares Legendre polynomial expansion, in which only the even-order terms contribute, given by

$$W(\theta) = A_0[1 + a_2 P_2(\cos\theta) + a_4 P_4(\cos\theta)], \qquad (1)$$

where the angular distribution coefficients a_2 and a_4 depend on the level spins, multipolarities, and mixing ratios (δ), and A_0 corresponds to the relative cross section of the γ ray. This fit is compared to the theoretical calculations of the angular distribution coefficients from the statistical model code CINDY [7] to determine δ values and level spins. The angular distribution of the 1268.8 keV γ ray from the 2485.1 keV 4_3^+ level to

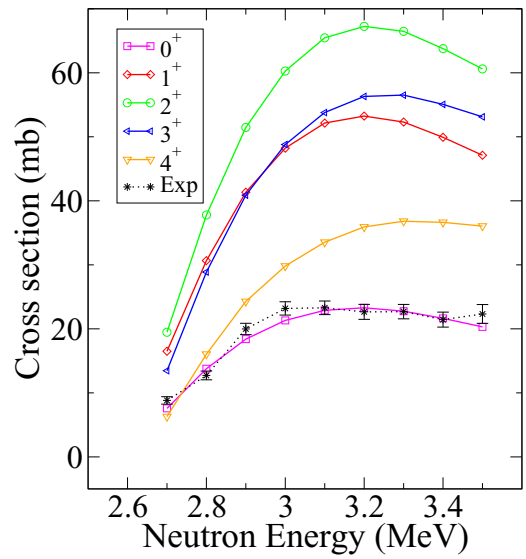

FIG. 2. Comparison of the measured relative cross section for the 2604.1 keV 0^+ state with the theoretical cross sections calculated with the code CINDY [7].

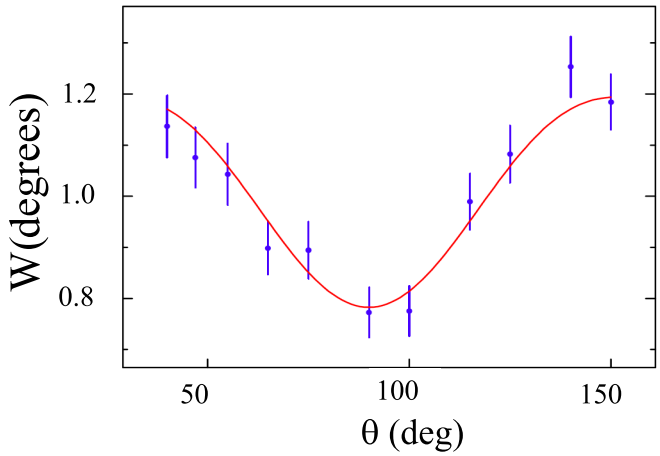

FIG. 3. Angular distribution of the 1268.8 keV γ ray from the 2485.1 keV 4_3^+ level to the 2_2^+ level.

the 2_2^+ state is shown in Fig. 3. Lifetimes of the excited levels were determined using the Doppler-shift attenuation method (DSAM) following the $(n, n'\gamma)$ reaction [8,9]. An example of the Doppler-shift of the 1268.8-keV γ ray from the keV level is shown in Fig. 4. The spectral fitting was performed using the TV software package [10].

In earlier work from our laboratory [11], it was shown that the size of the particles of the scattering sample material could affect the determination of the level lifetimes by DSAM with fast neutrons, with small particle sizes leading to erroneously shorter measured lifetimes. The scattering sample used in this study was investigated with x-ray powder diffraction, and the average particle size was determined to be about 20 nm, somewhat smaller than that employed in most of our measurements. At the energies of the angular distributions performed in this study, the ranges of the recoiling nuclei vary from about 19 to 26 nm, comparable to the average particle size. Thus there is some concern about how the particle size affects the measured lifetimes. One way to assess the effect of the particle size is to compare our measured lifetimes to those determined with other methods. Unfortunately, there are few known lifetimes from other measurements with which

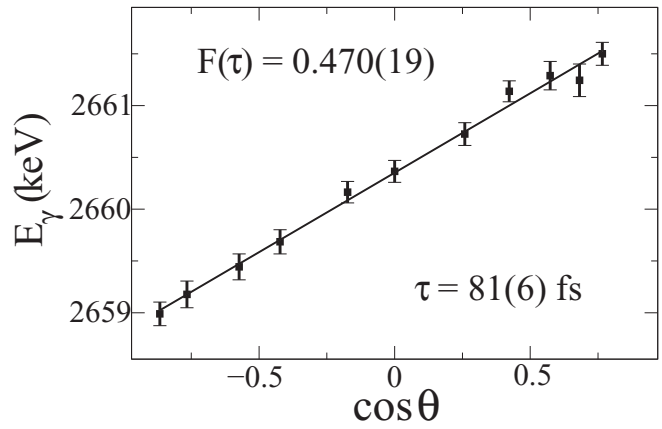

FIG. 4. Doppler-shift attenuation data for the 2660.4 keV γ ray from the 3219.4 keV level.

our extracted values can be compared. Many of the known lifetimes [4] are either too long to be determined with DSAM or they are from higher-spin states that are not populated in the $(n, n'\gamma)$ reaction. However, recent lifetime determinations with the (γ, γ') reaction for the 2951 and 3213 keV levels (τ = 109(19) and 15.7(5.5) fs, respectively [12]) are in reasonably good agreement with those measured in this work (τ = 150(16) and 16(2) fs, respectively).

III. EXPERIMENTAL RESULTS

The spectroscopic information obtained from the $(n, n'\gamma)$ measurements is summarized in Table I. For the levels below 2.2 MeV, the reported data are from the angular-distribution measurements with 2.4 MeV neutrons. For levels from 2.2 to 2.95 MeV, the measurements were made with 3.0 MeV neutrons; for higher-lying levels, the measurements were made with 3.7 MeV neutrons.

A. Previously reported levels not observed in the current study

Several levels, including some that are tentative in the Nuclear Data Sheets (NDS) compilation [4], were not observed and, therefore, are removed from the level scheme:

(i) *1881.2 keV (1,2,3) level*: The reported 665.0 keV γ ray from this level was not observed [4].

(ii) *2346.9 keV level*: Gamma rays of 466.5 and 1130.0 keV were tentatively reported from this level [4]. In our work, the 464.7 keV γ ray with a threshold of 3.3 MeV was assigned to a level at 3282.1 keV. The 1129.9 keV γ ray is from the 1689.0 keV level, as reported in Ref. [4], and is not a doublet.

(iii) *2363.0 keV (2^+, 3^+) level*: The 575.3 keV γ ray is reported as the most intense transition from the level [4]. We place this γ ray from the 1791.5 keV level, as reported in Ref. [4]; however, it is clearly not a doublet. The reported 1030.6 and 1805 keV γ rays were not observed in our spectra.

(iv) *2570 keV level*: We did not observe any of the γ rays from this reported level observed in a ^{77}Se(d, t) experiment [4], and hence it is not placed in our level scheme.

(v) *2605.7 keV level*: This level is reported in Ref. [4] with a 2046.6 keV γ ray to the 2_1^+ state. We rather observe a 2044.9 keV γ ray that has been placed from the 2604.1 keV 0^+ state.

(vi) *2630.8 keV (1,2) level*: This level is not included in the level scheme as the reported 942.3 keV γ ray has a threshold of 3.2 MeV, and the 2071.3 and 2627.0 keV γ rays are not present in our spectra.

(vii) *2691 keV (3^-) level*: The 2691 keV level was placed from the (p, p') reaction, but no transitions from this level are reported in Ref. [4]. No γ rays from a level at this energy were observed in our spectra, therefore this level is refuted.

(viii) *2853 keV (4^+) level*: We find no evidence for this level as observed in a (p, p') experiment [4].

TABLE I. Levels of ^{76}Se from the current $(n, n'\gamma)$ measurements. Transition probabilities are calculated for those levels whose lifetimes have been measured. Spins of the states (J_i^π), level energies (E_i), γ-ray energies (E_γ), average experimental attenuation factors $[\overline{F}(\tau)]$, level lifetimes (τ), branching ratios (BR), multipole mixing ratios (δ^+_- or πL), $B(E2)\downarrow$, $B(M1)\downarrow$, and $B(E1)\downarrow/B(E3)\downarrow$ values are listed. The δ value with the lower χ^2 is listed for values with asymmetric uncertainties; positive uncertainties are reported in the superscripts and negative uncertainties in the subscripts. Newly assigned E_γ's and τ's from the present measurements are in *italics*, with new levels in **bold**.

E_i (keV)	E_f (keV)	$J_i^\pi \to J_f^\pi$	E_γ (keV)	$\overline{F}(\tau)$	τ (fs)	BR	δ^+_- or πL	$B(E2)\downarrow$ (W.u.)	$B(M1)\downarrow$ (μ_N^2)	$B(E1)\downarrow/B(E3)\downarrow$ (mW.u.)/(W.u.)
559.10(4)	0.00	$2_1^+ \to 0_1^+$	559.10(2)		17.3(3)[a] ps	1	$E2$	44(1)[a]		
1122.27(8)	559.10	$0_2^+ \to 2_1^+$	563.19(3)		16(7)[a] ps	1	$E2$	47(22)[a]		
1216.23(8)	559.10	$2_2^+ \to 2_1^+$	657.09(3)		4.9(3)[a] ps	0.628(4)[a]	+5.2(2)[a]	43(3)[a]	0.00092(9)[a]	
	0.00	$2_2^+ \to 0_1^+$	1216.12(4)			0.372(4)[a]	$E2$	1.21(10)[a]		
1330.95(9)	559.10	$4_1^+ \to 2_1^+$	771.75(2)		2.19(7)[a] ps	1	$E2$	71(2)[a]		
1689.03(8)	1330.95	$3_1^+ \to 4_1^+$	358.25(17)		4.6^{17}_{9}[a] ps	0.029(2)	$+1.8^{10}_{12}$	35^{35}_{28}	0.002^{2}_{1}	
							$+0.8^{20}_{3}$	18^{35}_{8}	0.005^{2}_{5}	
	1216.23	$3_1^+ \to 2_2^+$	472.87(15)			0.325(3)	+0.41(5)	18(5)	0.03(1)	
							+5.4(9)	123^{64}_{54}	0.001(1)	
	559.10	$3_1^+ \to 2_1^+$	1129.85(10)			0.646(3)	+2.44(1)	2.8(8)	0.0008(2)	
1787.70(13)	1330.95	$2_3^+ \to 4_1^+$	456.98(12)	0.035(9)	1700^{600}_{350}[c]	0.018(1)[b]	$E2$	23(6)		
	1216.23	$2_3^+ \to 2_2^+$	571.50(6)			0.059(1)[b]	$+0.48^{73}_{22}$	4.5^{35}_{16}	0.009^{4}_{5}	
	1122.27	$2_3^+ \to 0_2^+$	665.65(14)[b]			0.190(1)[b]	$E2$	37(10)		
	559.10	$2_3^+ \to 2_1^+$	1228.51(6)			0.588(2)[b]	-0.52^{9}_{7}	1.1(3)	0.008(3)	
	0.00	$2_3^+ \to 0_1^+$	1787.56(8)			0.147(1)[b]	$E2$	0.2(1)		
1791.46(12)	1216.23	$0_3^+ \to 2_2^+$	575.30(4)			0.861(6)	$E2$			
	559.10	$0_3^+ \to 2_1^+$	*1232.24(8)*			0.139(6)	$E2$			
2026.08(8)	1330.95	$4_2^+ \to 4_1^+$	694.97(9)[b]		2.6(6)ps[a]	0.318(6)[b]	$+2.4^{10}_{6}$	28^{26}_{12}	0.003(2)	
							−0.36(15)	3.7^{14}_{9}	0.018^{7}_{4}	
	1216.23	$4_2^+ \to 2_2^+$	809.83(6)			0.649(6)[b]	$E2$	31^{9}_{6}		
	559.10	$4_2^+ \to 2_1^+$	1466.79(10)			0.032(2)[b]	$E2$	0.08(2)		
2127.30(12)	1791.46	$2_4^+ \to 0_3^+$	335.94(20)			0.035(2)				
	1787.70	$2_4^+ \to 2_3^+$	339.60(10)			0.106(2)				
	1689.03	$2_4^+ \to 3_1^+$	438.50(15)			0.243(4)				
	1216.23	$2_4^+ \to 2_2^+$	911.03(10)			0.025(2)				
	1122.27	$2_4^+ \to 0_2^+$	*1004.98(16)*			0.029(2)				
	559.10	$2_4^+ \to 2_1^+$	1568.07(12)			0.474(4)				
	0.00	$2_4^+ \to 0_1^+$	2127.21(8)			0.087(2)				
2170.75(12)	1216.23	$0_4^+ \to 2_2^+$	954.47(9)	*0.028(9)*	2100^{1500}_{600}	0.135(6)	$E2$	3.4(14)		
	559.10	$0_4^+ \to 2_1^+$	1611.63(8)			0.865(6)	$E2$	1.6(6)		
2262.77(18)	1330.95	$6_1^+ \to 4_1^+$	931.50(20)		890(100)[a]	1	$E2$	68(8)		
2429.17(9)	2026.08	$3_1^- \to 4_2^+$	403.07(12)		20(10) ps[a]	0.015(2)	$E1$			0.01^{1}_{0}
	1689.03	$3_1^- \to 3_1^+$	740.13(3)			0.078(2)	$E1$			0.01^{1}_{0}
	1216.23	$3_1^- \to 2_2^+$	1212.92(5)			0.854(4)	$E1$			0.01^{1}_{0}
	559.10	$3_1^- \to 2_1^+$	1870.04(4)			0.035(2)	$E1$			0.001(1)
	0	$3_1^- \to 0_1^+$	2429.21(6)			0.017(2)	$E3$			9^{9}_{3}
2485.07(10)	1689.03	$4_3^+ \to 3_1^+$	796.08(6)	0.087(10)	700^{110}_{90}	0.177(4)	$+0.20^{19}_{13}$	1.3^{3}_{2}	0.027(5)	
	1330.95	$4_3^+ \to 4_1^+$	1154.09(9)			0.600(6)	−0.35(5)	2.0(3)	0.028^{5}_{4}	
	1216.23	$4_3^+ \to 2_2^+$	1268.81(9)			0.223(5)	$E2$	4.0(6)		
2489.42(11)	1689.03	$5_1^+ \to 3_1^+$	800.40(9)		1.3^{4}_{3}[a] ps	0.667(4)[a]	$E2$	67(23)[a]		
	1330.95	$5_1^+ \to 4_1^+$	1158.45(5)			0.333(4)[a]	+2.9(8)[a]	4.7(17)[a]	0.0006(4)[a]	

TABLE I. (*Continued.*)

E_i (keV)	E_f (keV)	$J_i^\pi \to J_f^\pi$	E_γ (keV)	$\overline{F}(\tau)$	τ (fs)	BR	δ^+_- or πL	$B(E2)\downarrow$ (W.u.)	$B(M1)\downarrow$ (μ_N^2)	$B(E1)\downarrow/B(E3)\downarrow$ (mW.u.)/(W.u.)
2514.72(10)	1791.46	$2_5^+ \to 0_3^+$	*723.22(11)*	*0.036(12)*	1700^{570}_{340}	0.033(2)	$E2$	4(1)		
	1787.70	$2_5^+ \to 2_3^+$	727.05(3)			0.613(9)	+0.24(5)	4(1)	0.05(1)	
	1689.03	$2_5^+ \to 3_1^+$	*825.79(08)*			0.016(3)	-3_3^{18}	1_1^9	0.0001(1)	
							-1_1^{15}	0.5_4^{70}	0.0005(5)	
	1122.27	$2_5^+ \to 0_2^+$	1392.34(11)			0.012(3)	$E2$	0.06(1)		
	559.10	$2_5^+ \to 2_1^+$	1955.52(4)			0.325(7)	−0.57(7)	0.07(2)	0.0010(3)	
							-9_2^7	0.3_1^5	0.00002_2^1	
2604.12(12)	1216.23	$0_5^+ \to 2_2^+$	1387.86(6)	0.039(14)	1560^{920}_{430}	0.235(7)	$E2$	1.3(5)		
	559.10	$0_5^+ \to 2_1^+$	2044.93(6)			0.765(7)	$E2$	0.6(2)		
2617.95(10)	1787.70	$4_4^+ \to 2_3^+$	*830.41(11)*	*0.098(14)*	580^{110}_{80}	0.167(4)	$E2$	31(5)		
	1689.03	$4_4^+ \to 3_1^+$	928.82(14)			0.097(3)	$+8_5^{21}$	10_9^{45}	0.0002(2)	
							+0.15(11)	0.17(3)	0.010(2)	
	1330.95	$4_4^+ \to 4_1^+$	1286.91(10)			0.624(6)	−0.22(4)	0.6(2)	0.027(8)	
	1216.23	$4_4^+ \to 2_2^+$	*1401.70(11)*			0.112(4)	$E2$	1.5(3)		
2655.46(11)	1787.70	$1_1^- \to 2_3^+$	867.81(4)	*0.050(10)*	1180^{320}_{210}	0.159(3)	$E1$			0.11(2)
	1216.23	$1_1^- \to 2_2^+$	1439.15(6)			0.256(4)	$E1$			0.05(1)
	1122.27	$1_1^- \to 0_2^+$	1533.23(9)			0.023(2)	$E1$			0.0001(1)
	559.10	$1_1^- \to 2_1^+$	2096.20(4)			0.528(4)	$E1$			0.03(1)
	0	$1_1^- \to 0_1^+$	2655.45(7)			0.033(2)	$E1$			0.0001(1)
2669.98(10)	1787.70	$2_1^- \to 2_3^+$	882.21(5)	*0.046(10)*	1280^{390}_{240}	0.110(3)	$E1$			0.07(2)
	1689.03	$2_1^- \to 3_1^+$	980.90(3)			0.076(3)	$E1$			0.03(1)
	1216.23	$2_1^- \to 2_2^+$	1453.75(8)			0.224(6)	$E1$			0.03(1)
	559.10	$2_1^- \to 2_1^+$	2110.76(4)			0.590(4)	$E1$			0.03(1)
2805.18(12)	1330.95	$(4)^+ \to 4_1^+$	1474.21(15)	*0.099(19)*	560^{150}_{101}	1				
2812.11(14)	2429.17	$3_2^+ \to 3_1^-$	*382.92(17)*			0.126(5)	$E1$			
	1689.03	$3_2^+ \to 3_1^+$	*1123.07(10)*			0.155(5)	-1.61_{21}^{30}			
							−0.045(12)			
	1216.23	$3_2^+ \to 2_2^+$	1595.84(10)			0.563(6)	−0.03(3)			
	559.10	$3_2^+ \to 2_1^+$	*2252.92(12)*			0.155(6)	-1.0_2^{14}			
							-4.8_3^{10}			
2817.20(16)	1216.23	$(2) \to 2_2^+$	1600.92(6)	*0.310(13)*	*141(8)*	0.610(6)				
	559.10	$(2) \to 2_1^+$	2258.03(8)			0.390(6)				
2824.81(14)	2429.17	$5_1^- \to 3_1^-$	395.70(6)		8.9^{30}_{20} ps [a]	[e]	$E2$			
	2262.77	$5_1^- \to 6_1^+$	562.3(5) [d,a]				$E1$			
	2026.08	$5_1^- \to 4_2^+$	798.84(8)				$E1$			
	1330.95	$5_1^- \to 4_1^+$	1493.83(6)				$E1$			
2859.86(12)	2429.17	$4_1^- \to 3_1^-$	430.67(4)		[f]	0.364(6)	$+1.9_{13}^9$			
							$+0.7_2^{22}$			
	1689.03	$4_1^- \to 3_1^+$	*1170.86(8)*			0.186(5)	$E1$			
	1330.95	$4_1^- \to 4_1^+$	1528.86(9)			0.450(6)	$E1$			
2869.19(10)	1216.23	$2_6^+ \to 2_2^+$	1652.95(10)	*0.350(15)*	*118(8)*	0.295(6)	$+0.38_{12}^{14}$	1.1(1)	0.027(3)	
							$+1.1_8^3$	4.8_{28}^{14}	0.014_4^{10}	
	559.10	$2_6^+ \to 2_1^+$	2310.03(9)			0.579(6)	−0.52(9)	0.68(8)	0.018(2)	
							-12_6^{52}	3_2^{22}	0.0002(1)	
	0	$2_6^+ \to 0_1^+$	*2869.09(15)*			0.125(4)	$E2$	0.23(2)		
2917.38(15)	1330.95	$5_2^+ \to 4_1^+$	1586.41(8)	0.078(41)	720^{840}_{270}	1	+0.34(4)	0.6(3)	0.02(1)	

TABLE I. (*Continued.*)

E_i (keV)	E_f (keV)	$J_i^\pi \rightarrow J_f^\pi$	E_γ (keV)	$\overline{F}(\tau)$	τ (fs)	BR	δ^+_- or πL	$B(E2)\downarrow$ (W.u.)	$B(M1)\downarrow$ (μ_N^2)	$B(E1)\downarrow/B(E3)\downarrow$ (mW.u.)/(W.u.)
2950.10(14)	559.10	$1_1^+ \rightarrow 2_1^+$	2390.73(14)	0.299(24)	150(16)	0.367(8)	-0.2_1^{43}	0.04_1^5	0.010_{10}^1	
							-2.0_2^{25}	1_1^2	0.002_2^3	
	0	$1_1^+ \rightarrow 0_1^+$	2950.20(12)			0.633(8)	$M1$		0.010(1)	
2969.60(13)	2429.17	$4_2^- \rightarrow 3_1^-$	540.40(8)			0.325(9)	−0.44(12)			
							−1.7(4)			
	1689.03	$4_2^- \rightarrow 3_1^+$	1280.44(10)			0.675(9)	$E1$			
2974.86(14)	559.10	$3^{(+)} \rightarrow 2_1^+$	2415.62(12)			1				
3007.65(28)	1216.23	$2_7^+ \rightarrow 2_2^+$	1791.52(12)	0.656(17)	39(3)	0.089(5)	$+5_2^{58}$	5_3^{88}	0.001(1)	
							−0.21(19)	0.22(3)	0.021(3)	
	559.10	$2_7^+ \rightarrow 2_1^+$	2448.74(12)			0.868(7)	−0.16(5)	0.27(2)	0.083(8)	
	0	$2_7^+ \rightarrow 0_1^+$	3007.40(20)			0.043(7)	$E2$	0.20(1)		
3031.61(19)	1216.23	$0_6^+ \rightarrow 2_2^+$	1815.40(8)	0.341(21)	141(11)	0.377(12)	$E2$	5.8_7^9		
	559.10	$0_6^+ \rightarrow 2_1^+$	2472.39(12)			0.623(12)	$E2$	2.1(2)		
3045.86(22)	2824.81	$(5) \rightarrow 5_1^-$	221.21(11)	0.107(42)	570_{180}^{400}[g]	0.381(26)				
	1330.95	$(5) \rightarrow 4_1^+$	1714.72(10)			0.619(26)				
3069.53(20)	2127.30	$2^+ \rightarrow 2_4^+$	942.45(22)	*0.094(13)*	660_{90}^{120}	0.046(3)	-0.5_3^{47}	0.8_2^{26}	0.004_4^1	
							-12_7^{16}	4_3^9	0.00003_3^4	
	1689.03	$2^+ \rightarrow 3_1^+$	1380.34(16)			0.162(4)	+0.04(9)	0.003(1)	0.005(1)	
							-7_3^{14}	2_1^7	0.0001(1)	
	1216.23	$2^+ \rightarrow 2_2^+$	1853.07(14)			0.692(6)	+2.3(3)	1.7(6)	0.002(1)	
							$+0.003_{50}^{44}$	0.00002(1)	0.009(2)	
	559.10	$2^+ \rightarrow 2_1^+$	2510.49(15)			0.099(5)	$+1.3_{13}^{11}$	0.04(4)	0.0002(2)	
							$+0.3_3^{23}$	0.005_1^6	0.0005_5^1	
3083.59((22)	559.10	$(2,3)^+ \rightarrow 2_1^+$	2524.43(6)	*0.615(16)*	*47(3)*	1				
3105.22(11)	1330.95	$3^{(-)} \rightarrow 4_1^+$	*1774.35(18)*	0.190(14)	292(31)	0.205(6)				
	1216.23	$3^{(-)} \rightarrow 2_2^+$	*1888.70(22)*			0.225(5)				
	559.10	$3^{(-)} \rightarrow 2_1^+$	2546.20(10)			0.570(7)				
3159.63(28)	2669.95	$(2) \rightarrow 2_1^-$	489.68(28)			0.073(7)				
	2655.46	$(2) \rightarrow 1_1^-$	504.67(38)			0.068(6)				
	2429.17	$(2) \rightarrow 3_1^-$	730.58(25)			0.102(8)				
	2127.30	$(2) \rightarrow 2_4^+$	1032.52(10)			0.105(5)				
	1787.70	$(2) \rightarrow 2_3^+$	1372.33(22)			0.136(5)				
	1689.03	$(2) \rightarrow 3_1^+$	1470.87(23)			0.516(9)				
3160.85(12)	559.10	$0_7^+ \rightarrow 2_1^+$	2601.69(13)	0.111(37)	550_{150}^{300}	1	$E2$	0.7(3)		
3161.82(13)	2429.17	$3^- \rightarrow 3_1^-$	732.77(6)	0.148(25)	392_{62}^{91}	0.228(15)	$+0.2_1^{14}$	4.5_{10}^{30}	0.08_4^2	
	1330.95	$3^- \rightarrow 4_1^+$	1830.79(8)			0.290(10)	$E1$			0.07(1)
	1216.23	$3^- \rightarrow 2_2^+$	1945.48(10)			0.482(14)	$E1$			0.09(2)
3191.53(13)	1689.03	$3^+ \rightarrow 3_1^+$	*1502.54(11)*	*0.298(14)*	*162(11)*	0.635(20)	$+1.93_{24}^{28}$	17(4)	0.007(2)	
							−0.14(5)	0.42_3^4	0.06(1)	
	1330.95	$3^+ \rightarrow 4_1^+$	*1860.65(10)*			0.147(26)	-0.2_1^{88}	0.07_1^{17}	0.008_8^1	
	1216.23	$3^+ \rightarrow 2_2^+$	*1975.09(14)*			0.112(6)	−0.02(9)	0.00039(2)	0.0050(4)	
							-4.6_{14}^{33}	$0.9_{0.4}^{1.0}$	0.0002(1)	
	559.10	$3^+ \rightarrow 2_1^+$	*2632.39(13)*			0.106(6)	+0.26(10)	0.014(2)	0.0020(2)	
							$+14_8^{50}$	0.2_2^{11}	0.00001(1)	
3212.91(12)	559.10	$2^+ \rightarrow 2_1^+$	2653.80(10)	0.829(16)	16(2)	0.921(4)	$+3.2_4^7$	17_4^8	0.02(1)	
							−0.10(5)	0.18(2)	0.17(3)	
	0	$2^+ \rightarrow 0_1^+$	3212.78(11)			0.079(4)	$E2$	0.62_7^9		

TABLE I. (*Continued.*)

E_i (keV)	E_f (keV)	$J_i^\pi \rightarrow J_f^\pi$	E_γ (keV)	$\overline{F}(\tau)$	τ (fs)	BR	δ^+_- or πL	$B(E2)\downarrow$ (W.u.)	$B(M1)\downarrow$ (μ_N^2)	$B(E1)\downarrow/B(E3)\downarrow$ (mW.u.)/(W.u.)
3219.41(13)	2429.17	$3^{(+)}\rightarrow 3_1^-$	790.12(4)	*0.470(19)*	*81(6)*	0.332(8)				
	559.10	$3^{(+)}\rightarrow 2_1^+$	2660.36(8)			0.668(8)				
3230.43(12)	2170.75	$2^+\rightarrow 0_4^+$	1059.69(8)	0.065(49)	950^{3000}_{430}	1	$E2$	34^{28}_{26}		
3238.78(13)	2824.91	$(4^+)\rightarrow 5_1^-$	413.97(8)			1				
3263.01(11)	2127.30	$(3^-)\rightarrow 2_4^+$	1135.73(8)	0.188(52)	290^{140}_{80}	1				
3267.30(18)	1689.03	$(2,3)\rightarrow 3_1^+$	1578.24(19)	0.105(19)	570^{140}_{100}	0.030(5)				
	1330.95	$(2,3)\rightarrow 4_1^+$	1936.30(11)			0.418(9)				
	1216.23	$(2,3)\rightarrow 2_2^+$	2050.83(12)			0.200(8)				
	559.10	$(2,3)\rightarrow 2_1^+$	2708.34(10)			0.352(9)				
3282.14(14)	2817.20	$2^+\rightarrow (2)$	464.67(20)	0.322(19)	146(13)	0.336(9)				
	1122.27	$2^+\rightarrow 0_2^+$	2160.00(12)			0.664(9)	$E2$	4.1^4_3		
3295.24(12)	1787.70	$(1)\rightarrow 2_3^+$	1507.52(14)	0.427(17)	100(7)	0.124(7)				
	1122.27	$(1)\rightarrow 0_2^+$	2173.06(18)			0.055(8)				
	559.10	$(1)\rightarrow 2_1^+$	2736.21(10)			0.590(11)				
	0.00	$(1)\rightarrow 0_1^+$	3295.07(14)			0.231(8)				
3331.52(17)	559.10	$0_8^+\rightarrow 2_1^+$	2772.35(8)	0.169(23)	331^{61}_{51}	1	$E2$	0.8(1)		
3346.35(13)	2026.08	$(4)\rightarrow 4_2^+$	1320.57(18)			0.577(20)				
	1330.95	$(4)\rightarrow 4_1^+$	2015.13(14)			0.423(20)				
3348.64(20)	2170.73	$1(^+)\rightarrow 0_4^+$	1177.90(11)	0.110(86)	500^{2200}_{300}	1				
3351.54(29)	2669.95	$(1,2)^+\rightarrow 2^-$	681.44(32)	0.347(22)	130(13)	0.060(3)				
	1216.23	$(1,2)^+\rightarrow 2_2^+$	2135.40(20)			0.137(1)				
	559.10	$(1,2)^+\rightarrow 2_1^+$	2792.20(11)			0.803(4)				
3376.26(12)	0	$1,2^+\rightarrow 0_1^+$	*3376.29(12)*	*0.377(110)*	111^{71}_{42}	1				
3403.67(17)	2812.11	$(5^+)\rightarrow 3_2^+$	592.02(14)	0.607(27)	47(5)	0.453(19)				
	1330.95	$(5^+)\rightarrow 4_1^+$	2072.68(12)			0.567(19)				
3407.97(15)	2859.86	$(4)\rightarrow 4_1^-$	548.12(4)	0.081(41)	750^{810}_{270}	0.794(19)				
	1689.03	$(4)\rightarrow 3_1^+$	1718.93(10)			0.206(19)				
3435.96(34)	559.10	$2^+\rightarrow 2_1^+$	2876.40(28)	0.433(19)	91(7)	0.781(11)	$+0.64^{28}_{20}$	0.5(2)	0.014(3)	
	0.00	$2^+\rightarrow 0_1^+$	3436.28(20)			0.219(11)	$E2$	0.22(2)		
3441.28(17)	559.10	$(3^-)\rightarrow 2_1^+$	2882.11(22)			1				

[a]From the Nuclear Data Sheets [4].
[b]Mixed with a γ ray from another Se isotope, i.e., 665.65 keV γ ray with 666.27 keV γ ray from ^{80}Se and 694.97 keV γ ray with 694.92 keV γ ray from ^{78}Se. Branching ratios taken from Ref. [4].
[c]Differs from the Nuclear Data Sheets [4], discussed in Sec. III B.
[d]The 563 keV γ ray is a doublet and, therefore, the branching ratio has not been reported for the 2824.8 keV level.
[e]Branching ratios have not been reported as the 562 keV γ ray is a doublet and we do not observe the 335 keV transition from this level, reported in the Nuclear Data Sheets [4].
[f]Lifetime from Nuclear Data Sheets [4] of 1.73 ps, not observed in our measurement.
[g]Lifetime from Nuclear Data Sheets [4] is <0.28 ns.

(ix) *2911.0 keV (1 to 4) level*: The 548.0 keV γ ray tentatively reported from this level, observed in thermal neutron capture [4], has a threshold of 3.5 MeV and, therefore it has been excluded from the level scheme.

B. Newly reported levels and levels with new spectroscopic information

(i) *1787.7 keV 2_3^+ level*: The lifetime obtained for this level from our measurement, 1700^{+600}_{-350} fs, differs significantly from the reported value of 9^{+9}_{-3} ps [4]. The observed γ rays from the level have been assigned previously. The branching ratios reported in Table I are taken from Ref. [4] as the 665.7 keV γ ray to the 0_2^+ state is contaminated by the 666.7 keV $2_1^+\rightarrow 0_1^+$ γ ray in ^{80}Se. The $B(E2)$ value obtained for the $2_3^+\rightarrow 0_2^+$ transition is 37(10) W.u., and the level has been assigned to the 0_2^+ band. (See Sec. V A.)

(ii) *1791.5 keV 0_3^+ level*: This level was reported in Ref. [4] as questionable, but the present work

supports its existence with an additional 1232.2 keV branch to the 2_1^+ state. The isotropic angular distribution for the 575.3 keV γ ray to the 2_2^+ state and the excitation function data compared with CINDY calculations lead us to assign a spin-parity of 0^+.

(iii) *2127.3 keV* 2_4^+ *level*: A spin-parity of 2^+ is assigned to this level from the angular distributions and the excitation function. A 1005.0 keV γ ray to the 0_2^+ state has been assigned. The reported 796.1 keV transition to the 4_1^+ state [4] was not observed in the 2.4 MeV angular distribution data, and the threshold for this γ ray is 2.5 MeV. Thus, it has been reassigned to a level at 2485.1 keV.

(iv) *2170.8 keV* 0_4^+ *level*: A 382.9 keV γ ray was reported from this level [4] as observed in the (n, γ) reaction. However, it has threshold of 3.0 MeV and has been assigned to the 2812.1 keV level. In this work, the tentative spin-parity assignment in Ref. [4] of 0^+ has been confirmed.

(v) *2485.1 keV* 4_3^+ *level*: Observed for the first time in this work, this level decays to the 3_1^+, 4_1^+, and 2_2^+ states via 796.1, 1154.1, and 1268.8 keV γ rays, respectively. The angular distributions compared with CINDY calculations for both the 1154.1 and 1268.8 keV γ rays yield the lowest χ^2 value for spin 4 with a measurable mixing ratio indicating positive parity.

(vi) *2514.7 keV* 2_5^+ *level*: Additional 723.2 and 825.8 keV branches from this level to the 0_3^+ and 3_1^+ states, respectively, have been identified in this work. The tentative spin-parity assignment from Ref. [4] of 2^+ has been confirmed, and a newly measured level lifetime is reported in Table I.

(vii) *2604.1 keV* 0_5^+ *level*: New decays to the 2_2^+ and 2_1^+ states are observed as 1387.9 and 2044.9 keV γ rays, respectively. The excitation function (see Fig. 2) leads us to assign a spin-parity of 0^+.

(viii) *2618.0 keV* 4_4^+ *level*: This level, placed previously from an $(n, n'\gamma)$ reaction measurement [4], is reported with an energy of 2619.2 keV with a tentative spin-parity of $(4)^+$. In this work, we confirm the spin-parity to be 4^+, report the level lifetime as 580^{+110}_{-80} fs, and place additional 830.4 and 1401.7 keV γ rays to the 2_3^+ and 2_2^+ states, respectively. The $B(E2)$ of 31(5) W.u. to the 2_3^+ state supports its assignment to the 0_2^+ band. (See Sec. V A.)

(ix) *2655.5 keV* 1_1^- *level*: This level, with branches to the 2_3^+, 2_2^+, and 2_1^+ states, was previously observed in ^{76}As β^- decay [13]. Additional branches to the 0_2^+ and 0_1^+ levels are reported [4] and have been observed in this work; however, the reported 484.8 and 1324 keV γ rays to the 0_4^+ and 4_1^+ states [4], respectively, were not observed in our spectra. The 2655.5 keV γ ray, the lower energy member of a doublet with a threshold at 2.7 MeV, arises from this level, and the other member of the doublet, with a threshold near 3.3 MeV, shown in Fig. 5, comes from the 3212.9 keV level. The level lifetime obtained is 1180^{+320}_{-210} fs and other properties reported in Table I are from the 3.0 MeV angular distribution, which is close to the level energy and, therefore, complications from the other member of the doublet could be avoided. The angular distributions of the 2096.2 and the 1439.2 keV γ rays are supportive of a 1^- spin-parity assignment.

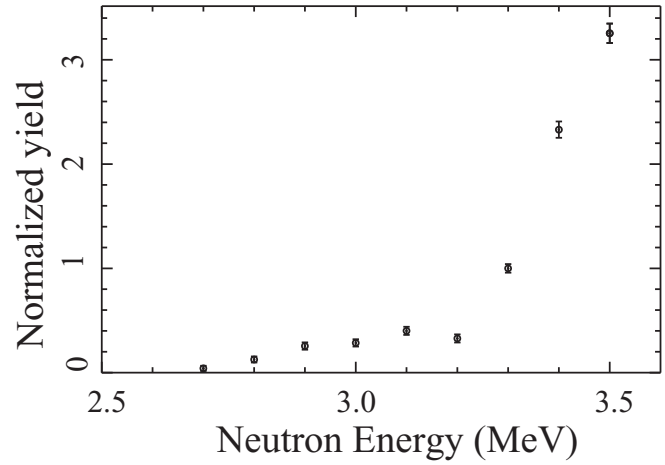

FIG. 5. Excitation function for the 2655 keV γ rays. The two distinct thresholds indicate a doublet.

(x) *2805.2 keV (4)* $^+$ *level*: The 1588.0 keV γ ray reported in Ref. [4] was not observed in our spectra. We obtain a level lifetime of 560^{+150}_{-101} fs.

(xi) *2812.1 keV* 3_2^+ *level*: This level was reported in Refs. [14,15], with only a branch to the 2_2^+ state and with no spin assigned. In this work, we observe additional 382.9, 1123.1, and 2252.9 keV γ rays to the 3_1^-, 3_1^+, and 2_1^+ states, respectively. The spin-parity has been confirmed to be 3^+.

(xii) *2817.2 keV (2) level*: We obtain a lifetime of 141(8) fs and could only assign a tentative spin of (2) for this level.

(xiii) *2869.2 keV* 2_6^+ *level*: This level was reported in the NDS [4] with a tentative spin assignment of (1 to 4). The measured lifetime for this level is 118(8) fs. Additional 1653.0 and 2869.1 keV transitions to the 2_2^+ and 0_1^+ states were observed; a spin-parity of 2^+ has been assigned in this work based on the angular distribution of the ground state transition.

(xiv) *2917.4 keV* 5_2^+ *level*: Only a 1586.4 keV γ ray to the 4_1^+ state with a $B(E2) < 1$ W.u. is observed.

(xv) *2969.6 keV* 4_2^- *level*: Observed for the first time, this 4_2^- level decays to the 3_1^- and 3_1^+ states with 540.4 and 1280.4 keV γ rays, respectively. The decay branches are similar to those of the 4_1^- level. We do not observe a transition to the 4_1^+ level.

(xvi) *2974.9 keV* $3^{(+)}$ *level*: A 2415.6 keV γ ray from the 2974.9 keV level populates the 2_1^+ state. A 2975.2 keV 6_2^+ state decaying to the 4_2^+ level via a 950 keV γ ray has been reported in Ref. [16].

A weak 950 keV γ ray with a threshold around 3.5 MeV is observed in the excitation function spectra; however, population of a 6^+ state with the inelastic neutron scattering (INS) reaction is unlikely at this excitation energy. Based on our observation we assign a spin-parity of $3^{(+)}$ to the newly observed 2974.9 keV level.

(xvii) *3007.7 keV* 2^+_7 *level*: The 3007.7 keV level decays to the 2^+_2, 2^+_1, and 0^+_1 states. The angular distribution of the ground state supports a spin-parity of 2^+.

(xviii) *3031.6 keV* 0^+_6 *level*: Observed here for the first time, the 3031.6 keV 0^+ level decays to the 2^+_2 and 2^+_1 states. The isotropic angular distributions for both γ rays along with the excitation function data lead us to assign a spin-parity of 0^+.

(xix) *3069.5 keV* 2^+ *level*: A spin of 2^+ has been assigned to this level from the angular distribution of the 1853.1 keV transition to the 2^+_2 state. The level lifetime for the state was found to be 660^{+120}_{-90} fs. Previously reported γ rays of 399.5, 897.0, and 3072.0 keV [4] were not observed in this work. The 942.5 keV γ ray reported in Ref. [16] from the 7^+ level has been observed with a threshold of 3.2 MeV, and it has been assigned to this level, in agreement with the NDS [4].

(xx) *3105.2 keV* $3^{(-)}$ *level*: Additional 1774.4 and 1888.7 keV γ rays to the 4^+_1 and 2^+_2 states, respectively, were placed and a lifetime of 292(31) fs is obtained for this level.

(xxi) *3160.9 keV* 0^+_7 *level*: In the NDS [4], the 2601.25 keV γ ray is reported as depopulating the 3160.1 keV level. We observe a 2601.7 keV γ ray from the 3160.9 keV level to the 2^+_1 level with an isotropic angular distribution. This level is therefore assigned a spin-parity of 0^+.

IV. SHELL MODEL CALCULATIONS

Similar to our study of ^{76}Ge [1], configuration interaction (CI) calculations in the $jj44$ model space (see the Appendix of Ref. [1]), consisting of the $0f_{7/2}$, $1p_{3/2}$, $1p_{1/2}$, and $0g_{9/2}$ orbitals for protons and neutrons, were performed using the shell model code NUSHELLX with the JUN45 and $jj44b$ Hamiltonians. The calculated $B(E2)$'s for all possible transitions between low-spin states in ^{76}Se are shown in Fig. 6 and the low-lying band structures are compared in Fig. 7. The first excited 0^+ band ($4^+_4 \rightarrow 2^+_3 \rightarrow 0^+_2$) is predicted well in both calculations; however, the calculated γ-band-like structure occurs at a much higher energy than is observed experimentally. Most notably, the first excited 3^+ state is calculated at an energy which is more than 1 MeV higher than the experimental energy.

V. DISCUSSION

Interpreting the low-lying structure of the stable Se nuclei is challenging with shape transitions, shape coexistence, and triaxiality in evidence. Following the identification of shape coexistence in ^{72}Se [17] and later in ^{74}Se [18], the identification of this phenomenon in other nuclei in this mass region has proliferated [19]. The defining feature of shape coexistence in even-even nuclei is generally regarded as the occurrence of a low-lying 0^+ excited state, which exhibits a structure decidedly different from the ground state. These low-lying structures have been identified in ^{72}Se and ^{74}Se, but were not quite as evident in ^{76}Se. In fact, it can be argued that ^{76}Se appears to be the most vibrational of these nuclei, with a candidate two-phonon (0^+, 2^+, 4^+) triplet of collective states. On the other hand, high-spin spectroscopic studies of this nucleus reveal a different picture, with well-developed bands

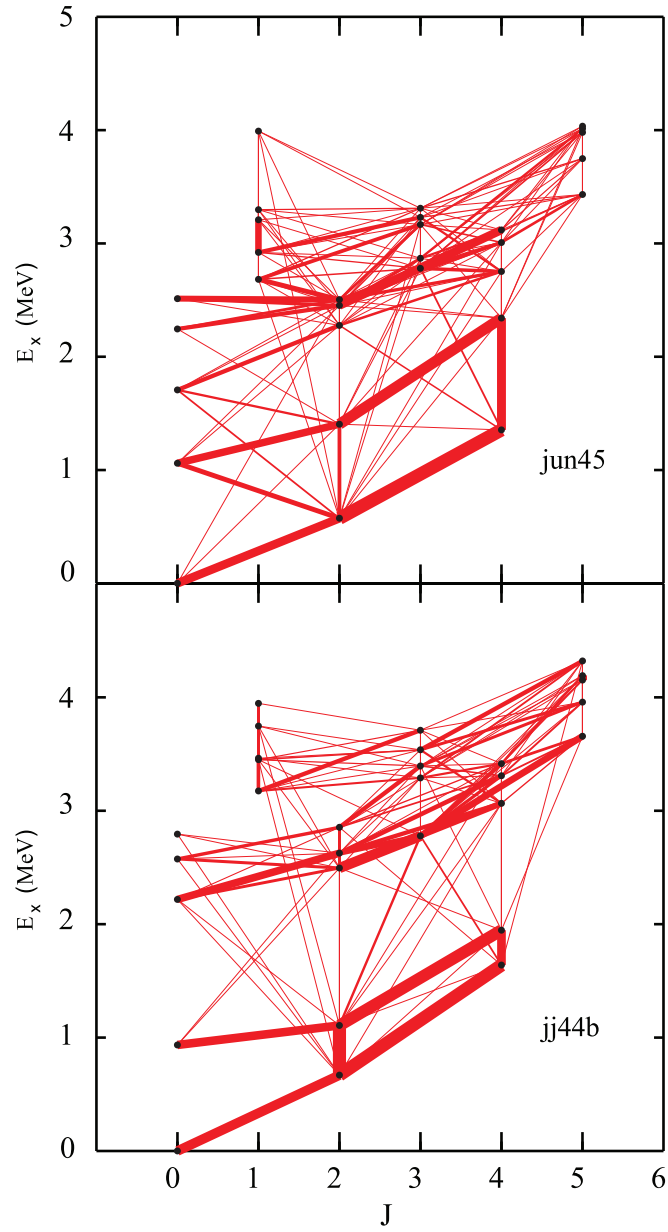

FIG. 6. Calculated levels in ^{76}Se connected by bars whose widths are proportional to the $B(E2)$ values obtained in the present shell model calculations. Only those transitions with a $B(E2)$ value larger than 1 W.u. are depicted in the figure.

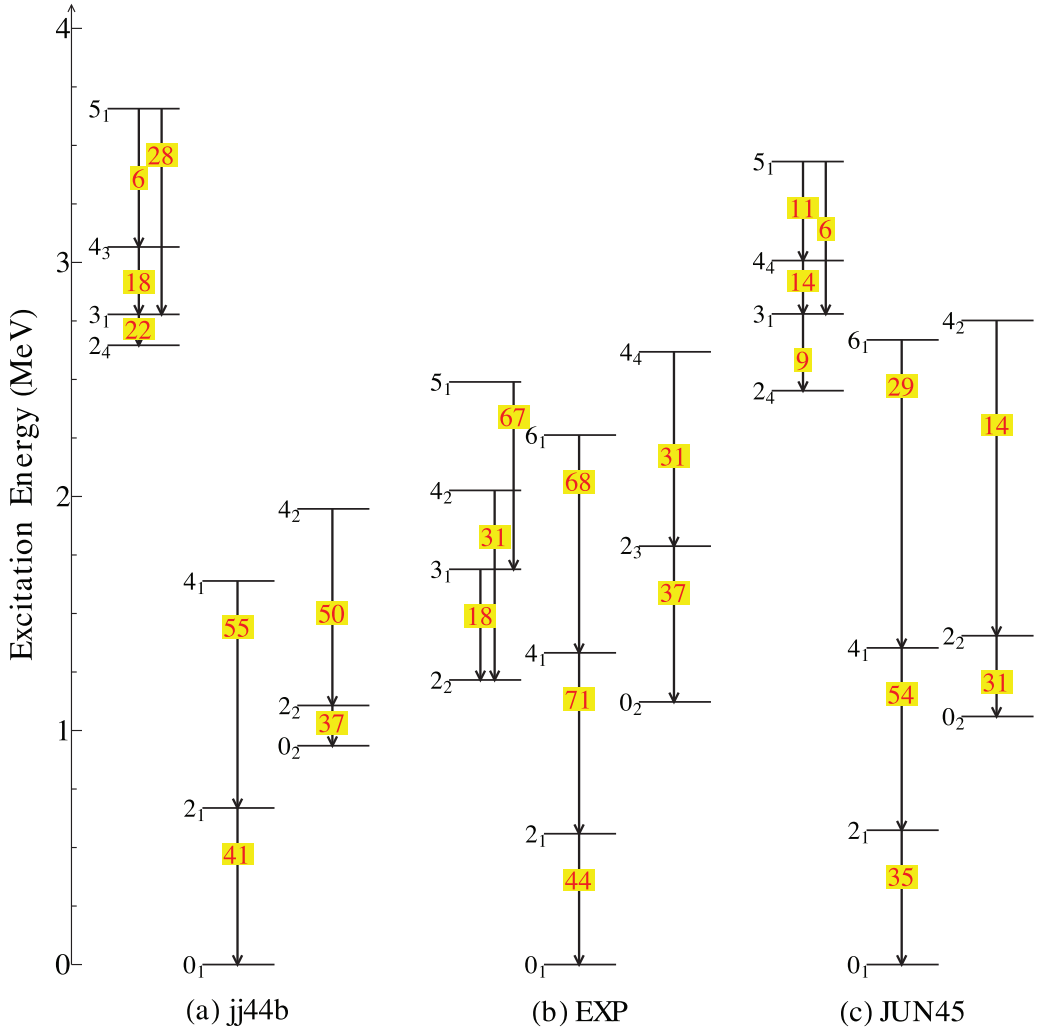

FIG. 7. Partial level scheme of positive-parity states in ^{76}Se from shell model calculations [(a) and (c)] and experiment [(b)] with $E2$ transition probabilities in W.u.

established to high angular momentum: the yrast (ground-state) band to (22^+) [20], the γ-vibrational band to (19^+) [20], and a negative-parity band [16]. In addition to these clearly collective excitations, we have identified and characterized a $4^+ \rightarrow 2^+ \rightarrow 0^+$ cascade of two $E2$ transitions, with $B(E2)$'s of 31(5) and 37(10) W.u., respectively, built on the first excited 0^+ state at 1122 keV. The picture for ^{76}Se thus differs from ^{72}Se and ^{74}Se, and indicates that the configuration mixing of this coexisting band is less than exhibited in the other Se nuclei.

Coulomb excitation provides direct information about the shape of the nucleus. Unfortunately, neither an older study of ^{76}Se by this method [21] nor a more comprehensive study [22] provide an unambiguous description of the nuclear structure. However, more recent studies of the stable even-mass isotones of ^{76}Se$_{42}$ contribute to our understanding of its low-spin structure. From Coulomb excitation of ^{74}Ge$_{42}$, it was concluded that the low-lying states cannot be interpreted as vibrational [23] and that the 0_2^+ state is a nearly spherical intruder. Similarly, ^{78}Kr$_{42}$ was found [24] to exhibit a prolate deformed ground-state band (and oblate deformation for the 2_2^+ state), but the structure of the 0_2^+ state is more difficult to assess. It appears that ^{76}Se is similar to its isotones (see Fig. 8) in displaying shape coexistence of prolate, oblate, and nearly spherical structures with significant mixing obscuring simplistic collective model interpretations. This mixing between coexisting structures modifies the experimental observables such as level energies, branching ratios, and transition rates.

Recently, IBM calculations with microscopic input from an energy density functional have been performed for a large range of Ge and Se nuclei [3], and the results indicate the coexistence of prolate and oblate, as well as spherical and γ-soft, shapes in the nuclei of this region. In this survey, detailed level properties are given for ^{76}Se, and a comparison between the available experimental data and these predictions, which include coexistence between spherical and γ-soft minima, is provided in Fig 9. The low energy of the γ band and the large $B(E2; 2_2^+ \rightarrow 2_1^+)$ suggest γ softness, and the small energy spacing of the 3_γ^+ and 4_γ^+ states is reminiscent of the γ-unstable rotor of Wilets and Jean [25]. Further, the prediction that the ground state of ^{76}Se is predominantly based

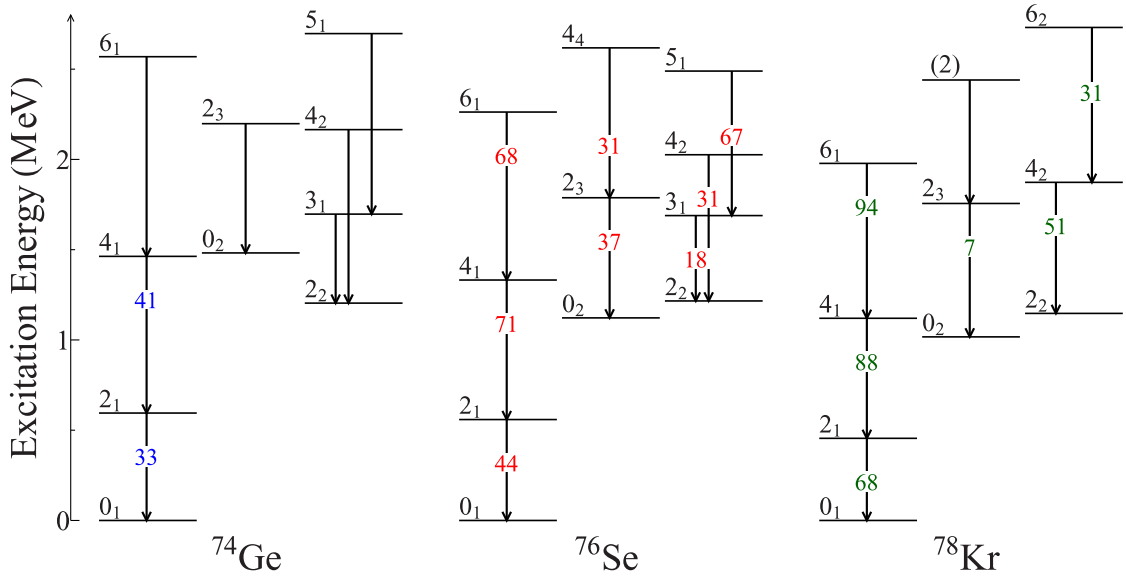

FIG. 8. Comparison of the low-lying positive-parity band structures in the $N = 42$ isotones ^{74}Ge [26], ^{76}Se, and ^{78}Kr [27]. The $E2$ transition strengths in W.u. for the intraband transitions are shown on the arrows.

on the deformed intruder configuration appears to be borne out by the larger energy spacing and smaller collectivity of the band built on the 0_2^+ excitation. Moreover, the theoretical and experimental $B(E2)$ strengths for the ground band, the 0_2^+ band, and the γ band agree well, as shown in Fig. 9.

A. Band structures in ^{76}Se

Ground band, 0_2^+ band, and γ band: From a fusion-evaporation reaction, Xu *et al.* [20] identified band structures with ground-band and γ-band structures to high spin in ^{76}Se. In this work, we have populated the low-lying ground band

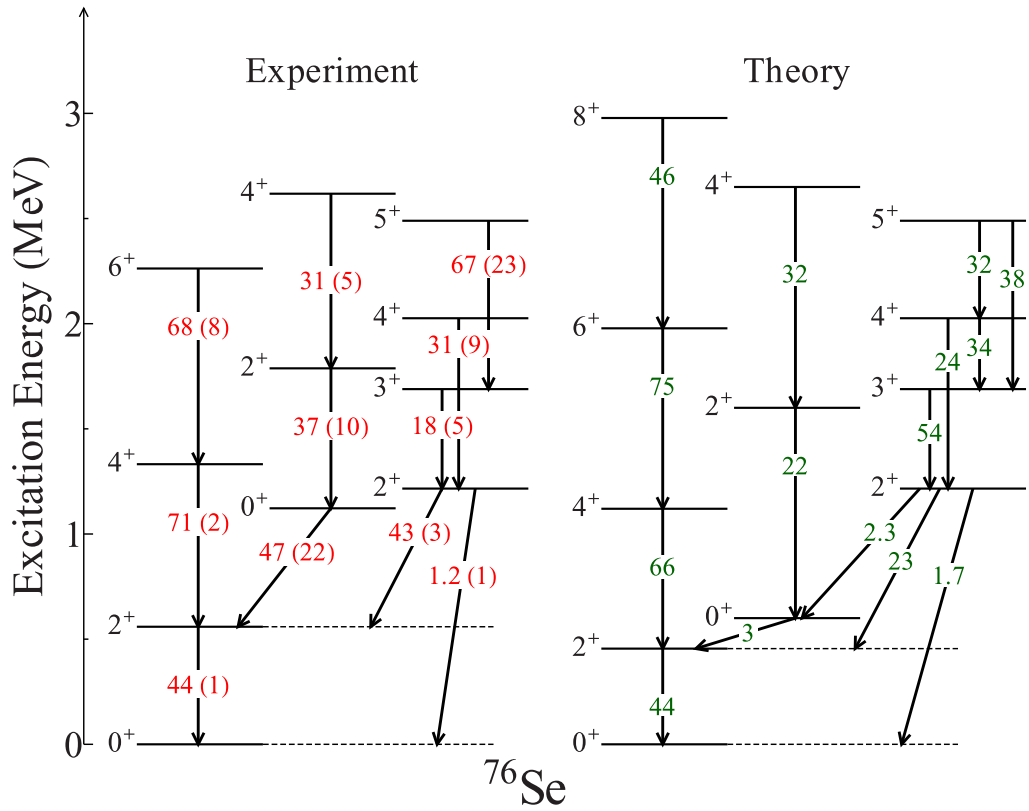

FIG. 9. Partial level of scheme of ^{76}Se, including $E2$ transition probabilities (W.u.) from IBM calculations [3] and experiment.

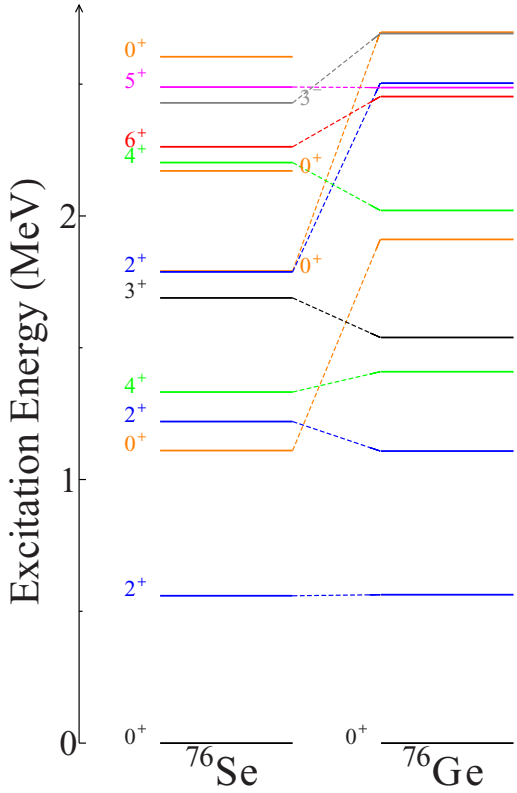

FIG. 10. Low-lying levels of ^{76}Se and ^{76}Ge [1] observed with the $(n, n'\gamma)$ reaction.

up to 6^+ and γ band up to 5^+. In addition, for the first time in ^{76}Se, we observe the band structure built on the excited 0^+ state at 1122.3 keV, shown in Fig. 8. The 2_3^+ state at 1787.7 keV and the 4_4^+ state at 2618.0 keV are the members of the 0_2^+ band. The $E2$ transition rates measured here support the findings of Xu *et al.* [20].

B. Comparison of ^{76}Se and ^{76}Ge

A comparison between the low-lying levels of ^{76}Se and ^{76}Ge observed with the $(n, n'\gamma)$ reaction is shown in Fig. 10. The 0_2^+ state of ^{76}Ge is at a much higher energy than in ^{76}Se, and a γ band [1] exists in both nuclei. ^{76}Se exhibits shape coexistence even at low energy but this phenomenon is not evident in ^{76}Ge. Transition strengths for the ground-state bands in ^{76}Se and ^{76}Ge are listed in Table II. The ^{76}Se transitions are slightly more collective in nature, and we can conclude that the ^{76}Se ground state is more deformed than ^{76}Ge.

TABLE II. $B(E2)\downarrow$ transition strengths in W.u, for the ground-state bands in ^{76}Se and ^{76}Ge [1].

$B(E2; i_1^+ \rightarrow f_1^+)$	^{76}Se	^{76}Ge
$B(E2; 2_1^+ \rightarrow 0_1^+)$	44(1)	29(1)
$B(E2; 4_1^+ \rightarrow 2_1^+)$	71(2)	38(9)
$B(E2; 6_1^+ \rightarrow 4_1^+)$	68(8)	91^{+55}_{-48}

VI. CONCLUSION

We investigated the low-lying, low-spin levels of ^{76}Se with the $(n, n'\gamma)$ reaction and characterized the level properties. For the first time, we established the 0_2^+ band, which supports shape co-existence in ^{76}Se predicted by large-scale shell model calculations and the interacting boson model [3]. ^{76}Ge is a favorable candidate for the observation of neutrinoless double$-\beta$ decay and this work establishes a comprehensive level scheme up to near 3 MeV for ^{76}Se, the daughter nuclide. From the $B(E2)$ transition strengths, we observe different deformations for ^{76}Ge and ^{76}Se.

ACKNOWLEDGMENTS

We wish to thank H. E. Baber for his many contributions to these measurements. This material is based upon work supported by the US National Science Foundation under Grant No. PHY-1606890. The enriched isotope used in this research was supplied by the United States Department of Energy Office of Science by the Isotope Program in the Office of Nuclear Physics. The figures for this article have been created using the LEVELSCHEME scientific figure preparation system [28].

[1] S. Mukhopadhyay, B. P. Crider, B. A. Brown, S. F. Ashley, A. Chakraborty, A. Kumar, M. T. McEllistrem, E. E. Peters, F. M. Prados-Estévez, and S. W. Yates, Phys. Rev. C **95**, 014327 (2017).
[2] J. Engel and J. Menéndez, Rep. Prog. Phys. **80**, 046301 (2017).
[3] K. Nomura, R. Rodríguez-Guzmán, and L. M. Robledo, Phys. Rev. C **95**, 064310 (2017).
[4] B. Singh, Nucl. Data Sheets **74**, 63 (1995).
[5] B. A. Brown and W. D. M. Rae, Nucl. Data Sheets **120**, 115 (2014).
[6] P. E. Garrett, N. Warr, and S. W. Yates, J. Res. Natl. Inst. Stand. Technol. **105**, 141 (2000).
[7] E. Sheldon and V. C. Rogers, Comput. Phys. Commun. **6**, 99 (1973).
[8] T. Belgya, G. Molnár, and S. W. Yates, Nucl. Phys. A **607**, 43 (1996).
[9] K. B. Winterbon, Nucl. Phys. A **246**, 293 (1975).
[10] A. Fitzler, TV User-Manual, Institute for Nuclear Physics, University of Cologne, 2000.
[11] E. E. Peters, A. Chakraborty, B. P. Crider, B. H. Davis, M. K. Gnanamani, M. T. McEllistrem, F. M. Prados-Estévez, J. R. Vanhoy, and S. W. Yates, Phys. Rev. C **88**, 024317 (2013).
[12] N. Cooper, F. Reichel, V. Werner, L. Bettermann, B. Alikhani, S. Aslanidou, C. Bauer, L. Coquard, M. Fritzsche, Y. Fritzsche, J. Glorius, P. M. Goddard, T. Möller, N. Pietralla, M. Reese, C. Romig, D. Savran, L. Schnorrenberger, F. Siebenhühner, V. V. Simon, K. Sonnabend, M. K. Smith, C. Walz, S. W. Yates,

O. Yevetska, and M. Zweidinger, Phys. Rev. C **86**, 034313 (2012).
[13] C. B. Zamboni and R. N. Saxena, Phys. Rev. C **39**, 2379 (1989).
[14] Y. Tokunaga, H. Seyfarth, O. Schult, H. Börner, C. Hofmeyr, G. Barreau, R. Brissot, U. Kaup, and C. Mönkemeyer, Nucl. Phys. A **411**, 209 (1983).
[15] M. Borsaru, D. Gebbie, J. Nurzynski, C. Hollas, L. Barbopoulos, and A. Quinton, Nucl. Phys. A **284**, 379 (1977).
[16] T. Matsuzaki and H. Taketani, Nucl. Phys. A **390**, 413 (1982).
[17] J. H. Hamilton, A. V. Ramayya, W. T. Pinkston, R. M. Ronningen, G. Garcia-Bermudez, H. K. Carter, R. L. Robinson, H. J. Kim, and R. O. Sayer, Phys. Rev. Lett. **32**, 239 (1974).
[18] R. Ronningen, A. Ramayya, J. Hamilton, W. Lourens, J. Lange, H. Carter, and R. Sayer, Nucl. Phys. A **261**, 439 (1976).
[19] K. Heyde and J. L. Wood, Rev. Mod. Phys. **83**, 1467 (2011).
[20] C. Xu, X. Q. Li, J. Meng, S. Q. Zhang, H. Hua, S. Y. Wang, B. Qi, C. Liu, Z. G. Xiao, H. J. Li, L. H. Zhu, Z. Shi, Z. H. Li, Y. L. Ye, D. X. Jiang, J. J. Sun, Z. H. Zhang, Y. Shi, P. W. Zhao, Q. B. Chen, W. Y. Liang, R. Han, C. Y. Niu, C. G. Li, C. G. Wang, Z. H. Li, S. M. Wyngaardt, R. A. Bark, P. Papka, T. D. Bucher, A. Kamblawe, E. Khaleel, N. Khumalo, E. A. Lawrie, J. J. Lawrie, P. Jones, S. M. Mullins, S. Murray, M. Wiedeking, J. F. Sharpey-Schafer, S. N. T. Majola, J. Ndayishimye, D. Negi, S. P. Noncolela, S. S. Ntshangase, O. Shirinda, P. Sithole, M. A. Stankiewicz, J. N. Orce, T. Dinoko, J. Easton, B. M. Nyakó, and K. Juhász, Phys. Rev. C **91**, 061303 (2015).
[21] J. Barrette, M. Barrette, G. Lamoureux, S. Monaro, and S. Markiza, Nucl. Phys. A **235**, 154 (1974).
[22] A. Kavka, C. Fahlander, A. Bäcklin, D. Cline, T. Czosnyka, R. Diamond, D. Disdier, W. Kernan, L. Kraus, I. Linck, N. Schulz, J. Srebrny, F. Stephens, L. Svensson, B. Varnestig, E. Vogt, and C. Wu, Nucl. Phys. A **593**, 177 (1995).
[23] Y. Toh, T. Czosnyka, M. Oshima, T. Hayakawa, H. Kusakari, M. Sugawara, Y. Hatsukawa, J. Katakura, N. Shinohara, and M. Matsuda, Eur. Phys. J. A **9**, 353 (2000).
[24] F. Becker, A. Petrovici, J. Iwanicki, N. Amzal, W. Korten, K. Hauschild, A. Hurstel, C. Theisen, P. Butler, R. Cunningham, T. Czosnyka, G. de France, J. Gerl, P. Greenlees, K. Helariutta, R.-D. Herzberg, P. Jones, R. Julin, S. Juutinen, H. Kankaanpää, M. Muikku, P. Nieminen, O. Radu, P. Rahkila, and C. Schlegel, Nucl. Phys. A **770**, 107 (2006).
[25] L. Wilets and M. Jean, Phys. Rev. **102**, 788 (1956).
[26] B. Singh and A. R. Farhan, Nucl. Data Sheets **107**, 1923 (2006).
[27] A. R. Farhan and B. Singh, Nucl. Data Sheets **110**, 1917 (2009).
[28] M. A. Caprio, Comput. Phys. Commun. **171**, 107 (2005); http://scidraw.nd.edu/levelscheme